Electron liquids and solids in one dimension

Vikram V. Deshpande[1], Marc Bockrath[2], Leonid I. Glazman[3] & Amir Yacoby[4]

Even though bulk metallic systems contain a very large number of strongly interacting electrons, their properties are well described within Landau's Fermi liquid theory of non-interacting quasiparticles. Although many higher-dimensional systems can be successfully understood on the basis of such non-interacting theories, this is not possible for one-dimensional systems. When confined to narrow channels, electron interaction gives rise to such exotic phenomena as spin–charge separation and the emergence of correlated-electron insulators. Such strongly correlated electronic behaviour has recently been seen in experiments on one-dimensional carbon nanotubes and nanowires, and this behaviour challenges the theoretical description of such systems.

According to Landau's Fermi liquid theory[1], a bulk metallic system of interacting electrons has low-energy excitations called quasiparticles that behave much like weakly interacting fermions. Therefore, many experiments on such systems can be understood on the basis of theories of non-interacting quasiparticles. The theoretical picture is qualitatively different in materials in which the electrons are confined to one-dimensional (1D) channels, or wires. In such wires, interactions cause electrons to behave in a highly cooperative way, and the Fermi liquid theory no longer applies. Progress in obtaining 1D materials realized as individual nanostructures has provided highly tunable systems that allow the study of the effects of interactions in many-electron systems. Other 1D tunable systems, such as those based on cold atoms[2,3], are also being developed and keep producing interesting results (see, for example, refs 4 and 5).

Here, we discuss the many ways in which interacting electrons in one dimension often produce surprising results that illuminate the role of the dimension of an interacting many-body system. After discussing the basic manifestations of 1D cooperative electron behaviour in simple tunnelling experiments, we focus on a number of new developments in 1D physics both in theory and in experiments on nanowires and carbon nanotubes. We first discuss the 1D phenomenon of spin–charge separation and experiments to observe it using the technique of momentum-conserved tunnelling between parallel nanowires[6,7]. The same kind of experiment raises the question of how a charge with a definite momentum is accommodated in a correlated 1D system[8]; this question is discussed in a section devoted to the apparent charge 'break-up'. The above physics can be understood using a theory valid at sufficiently low energies; however, the question of how 1D systems behave at higher energies is interesting as well. We discuss the recently developed 'nonlinear Luttinger liquid' theory addressing this question[9–13] and possible experiments aimed at its verification.

The availability of clean, freely suspended carbon nanotubes has enabled experiments to be performed in the low-electron-density regime. We discuss this limit, in which electrons organize themselves in a state of electron matter resembling a solid rather than a liquid[14]. Finally, we discuss recent observations of electrons in carbon nanotubes showing behaviour similar to that of a Mott insulator[15], which is a special kind of insulating state induced by electron–electron interactions.

From Fermi liquids to Luttinger liquids

Coulomb forces acting between electrons and ions hold in place the atoms forming a metal and ultimately determine the low-energy spectra of its elementary excitations, electrons in conduction bands and phonons. Despite the strength of the Coulomb forces (the corresponding energy is in the range of 10 eV), the classification of the low-energy excitations, suggested by Landau's Fermi liquid theory[1], is remarkably universal. In the language of this theory, the electric charge carriers in a conventional metal can be viewed as almost-free quasiparticles with Fermi statistics, the Coulomb interaction ultimately determining the crystalline structure of a material and the specific form of the quasiparticles' dispersion relationship (their energy–momentum relationship). The residual interaction between quasiparticles, stemming from the Coulomb repulsion, leads to the quasiparticle states having a finite energy uncertainty; the uncertainty for a given quasiparticle, however, is small in comparison with its energy.

Box 1 | Luttinger liquid and bosonization in one dimension

In our discussion about the inapplicability of the Fermi liquid theory to describe 1D interacting electron systems, shifts of the electron fluid have a crucial role. The creation of a particle at some point, x, along the wire may be viewed as a result of a shift of all the fluid to the left, say, of x by the interparticle distance, while the fluid to the right of x stays put; the 'bump' of density created at point x in this way will contain just one extra particle. The displacements of the fluid may be viewed as a superposition of harmonic waves. The quantized displacement waves are bosons that can be thought of as quanta of sound waves. At low energies, the interaction between bosons can be disregarded, which allows a low-energy excitation of a 1D fluid to be considered a collection of free bosons.

In one dimension, it is the above-mentioned bosons, rather than the Fermi quasiparticles of the Fermi liquid theory, that are the well-defined elementary excitations. This simple representation of the low-energy excitations of a 1D many-body quantum system is known as a Luttinger liquid. The lower the energy scale, the better this representation is supposed to work. It becomes exact for the so-called Tomonaga–Luttinger model[38,75,76], which is an idealized system of interacting fermions with a linear dispersion relation (this may be pictured as a model of electrons with some fixed Fermi velocity but with an infinitely deep conduction band). The operator that creates an electron at point x in a Luttinger liquid is, in the 'bosonized' representation, proportional to an operator that causes the finite displacement of a huge portion (one-half) of the liquid. Thus, in terms of the bosonic variables, the electron operator is a very non-local one. That inconvenience is a small price to pay to be able to recast a Hamiltonian of interacting electrons in the form of non-interacting particles[38,75,76] (bosons).

[1]Department of Physics, Columbia University, New York, New York 10027, USA. [2]Department of Physics and Astronomy, University of California, Riverside, California 92521, USA. [3]Departments of Physics and Applied Physics, Yale University, New Haven, Connecticut 06520, USA. [4]Department of Physics, Harvard University, Cambridge, Massachusetts 02138, USA.

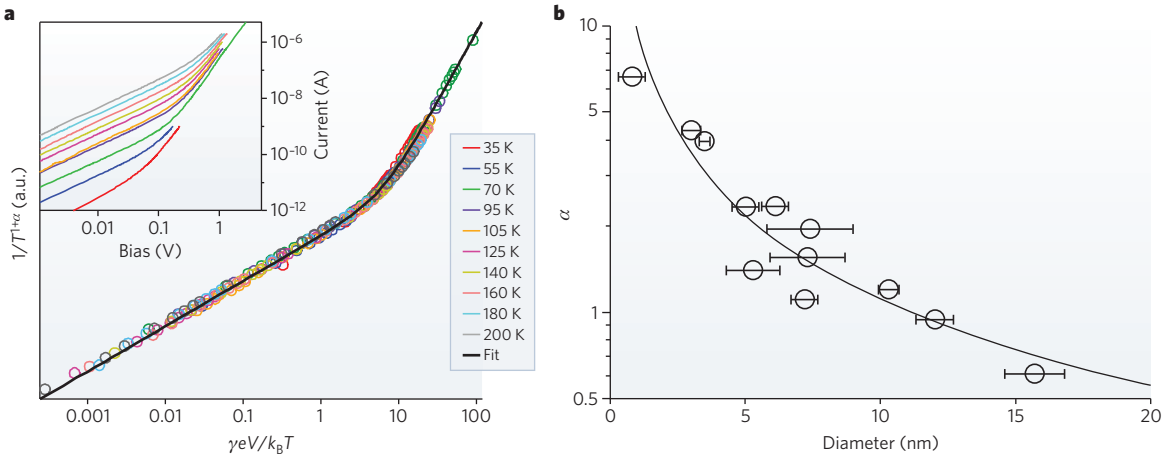

Figure 1 | Power-law behaviour of electron tunnelling with energy for molybdenum selenide wires of various diameters. **a**, Current–voltage data at different temperatures, T, for a molybdenum selenide wire bundle, scaled to a universal curve. Inset, the same data, but unscaled[29]. The parameter γ is a constant that indicates how the voltage drop across the device is shared between wire segments in series between the electrodes. a.u., arbitrary units; e, elementary charge; k_B, Boltzmann constant. **b**, Power-law exponent, α, as a function of wire diameter; $1/\alpha$ scales as the square root of the number of channels, in agreement with theory[19]. Error bars, diameter uncertainty. (Figure reproduced, with permission, from ref. 29.)

Although Landau's Fermi liquid theory provides a satisfactory account of bulk three-dimensional (3D) metals, the situation is qualitatively different in materials in which the electrons are confined to channels that are narrow relative to the electron wavelength and as a result effectively act as 1D wires for the electrons. Because the electrons are constrained to move in only two directions, right or left along the wire, any perturbations will affect a large number of electrons collectively. For instance, a charged particle trying to tunnel into the wire may create a short-wavelength density perturbation, forcing the liquid of interacting electrons to shift quickly away from the incoming particle. To accommodate the extra particle, however, ultimately all electrons to the left of it must shift by one-half of the average interparticle distance along the wire — in analogy to displacing equidistant beads on a string to make room for an additional bead. Likewise, all liquid to the right of the tunnelling particle must shift to the right by the same amount. This is in contrast to the 3D case, in which the charge of an incoming particle is compensated by a swift redistribution of the itinerant electrons, which are free to move away from the incoming electron in all directions, thus causing less of a collective disturbance of the so-called Fermi sea of electrons.

An immediate consequence of this intuitive implication of the role of collective behaviour when confining charged particles to one dimension is that the tunnelling rate for particles entering a 1D wire is suppressed around zero bias — the so-called zero-bias anomaly. By contrast, the tunnelling rate into a clean, conventional 3D metal is featureless (neither suppressed nor enhanced) at zero bias, confirming the unimpeded creation of particles or holes close to the Fermi level. This qualitative picture of tunnelling into a 1D electron system can be quantified within the so-called Luttinger liquid theory, 'bosonization' being a practical tool that makes the theory remarkably simple (Box 1).

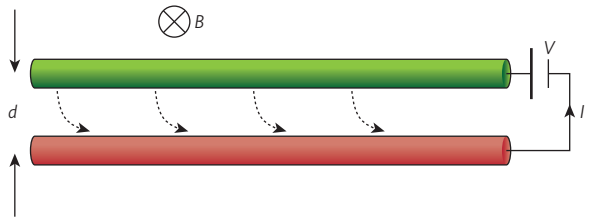

Figure 2 | Momentum-resolved tunnelling spectroscopy using two parallel wires. Electrons or holes tunnelling (arrows) between two parallel wires a distance d apart. The momentum boost in the tunnelling event, $\Delta p = edB$, is achieved by application of a magnetic field, B, perpendicular to the wires (into the page in this example). The energy resolution is achieved by controlling the interwire bias, V.

In experiments, the zero-bias anomaly can be observed in the differential conductance, dI/dV, where I is the current and V the voltage, of a tunnel junction attached to a 1D wire; a signature of Luttinger liquid behaviour would be a deep minimum at zero bias ($V = 0$). This discussion also applies to tunnelling into (or from) an end of a wire. The only difference is that now the electron liquid must shift away from the end by the entire interparticle distance; tunnelling is therefore suppressed more strongly.

A specific signature of Luttinger liquid behaviour predicted by theory[16–19] is that the zero-bias anomalies of dI/dV for tunnelling into a point at an end or into a point within the 'bulk' of a wire take the form of a power law in V (ref. 16): $dI/dV \approx V^{\alpha}$. Similarly, the temperature dependence of the tunnelling conductance at small, fixed bias also must follow a power law. The exponent α depends on the inter-electron interaction strength and the number of channels[19]. The quantization of electron motion across the wire's width results in the wire having a finite number of channels. The wider the wire, the larger the number of channels and the smaller the electron shift necessary to accommodate an extra electron, leading to the decrease of α towards zero (the conventional case of tunnelling into a clean conductor in higher dimensions).

These power-law dependences were specifically predicted for[17,18], and measured in, carbon nanotubes, for tunnelling both into an end and into the bulk[20–22]. The experimental results[20–22], notwithstanding the difficulties in interpretation associated with the finite-size effects and zero-bias anomalies in the resistive leads[23–25], are considered to be a clear manifestation of Luttinger liquid physics. Further confirmation of the Luttinger liquid behaviour came from resonant tunnelling experiments with gallium-arsenide-based quantum wire dots[26] and nanotube dots[27], nanotube capacitance measurements[28] and molybdenum selenide nanowires that allow variation of the number of channels available for electron motion[29] (Fig. 1).

Despite the agreement between the tunnelling anomaly measurements and theory, sceptics may consider it to be circumstantial evidence of the unusual behaviour of electrons associated with their confinement to one dimension. Indeed, the presence of disorder typical for highly resistive, conventional (non-1D) conductors also impedes the spreading of charge of tunnelling electrons. Because both Luttinger liquids and such higher-dimensional systems display a zero-bias anomaly[23–25], perhaps the proposed effect could be confused with the zero-bias anomaly in resistive leads. It would help to know the range of biases over which the power law for tunnelling conductance is expected to hold. An experiment on multiwalled carbon nanotubes produced results hardly distinguishable from the hallmark experiments[20–22], with a power law observed over a

Box 2 | Spin density waves in a Luttinger liquid

Electron fluids support waves of spin density, as well as waves of charge density. To see this, first consider a free-fermion gas, neglecting the interparticle interaction. Imagine that in some portion of the 1D system, an excess of spin-up particles is created and is compensated, so as to maintain charge neutrality, by the deficit of spin-down ones (the up–down axis in spin space may be picked arbitrarily). Even if the total density of particles remains unchanged, the energy of the system will increase, as locally the chemical potentials of the spin-up and spin-down particles deviate from the common equilibrium value. This energy increase provides the stiffness that defines the speed of the spin mode. In the free-fermion gas, the speeds of mass density and spin density modes both equal the Fermi velocity. The phases of oscillations of the local Fermi levels of the spin-up and spin-down electrons are opposite to each other and thus have no effect on the charge density (see figure, where $E_{F\uparrow}$ is the Fermi energy for spin-up electrons, $E_{F\downarrow}$ is the Fermi energy for spin-down electrons and x denotes position along the wire). Therefore, a spin wave does not create a perturbation of charge density,

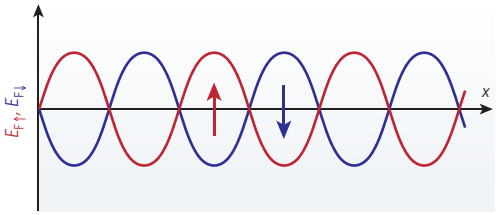

and a weak but long-range charge–charge interaction hardly affects the spin velocity, v_s, but increases the velocity of the charge mode, v_ρ. Note that the presence of interactions makes the waves of charge and spin truly collective excitations: they propagate with different velocities and therefore cannot be associated with a motion of a single particle endowed with the two qualities. The accommodation of a tunnelled electron requires charge and spin displacements, which propagate along the electron fluid with unequal velocities.

suspiciously wide range of biases[30]. Another uncertainty comes from the limitations caused by finite-size effects in the first experiments[20–22], which, for example, made it impossible to distinguish between the conducting and insulating states of a nanotube in the limit of very low temperatures. The possibility of 'dielectrization', that is, formation of an insulating state with a gap in the electron spectrum at low energies, was considered theoretically[18,31–34]. The single-point tunnelling phenomena described above gave only the first glimpse into the behaviour of electrons confined to one dimension.

Spin–charge separation

Another distinct manifestation of the correlated behaviour of electrons when confined to one dimension is the phenomenon of spin–charge separation. The electron liquid, along with the waves of electron charge density, supports waves of electron spin density. These are collective excitations, propagating with two different velocities (Box 2).

The successful observation and direct visualization of spin–charge separation has been achieved in experiments on so-called momentum-resolved tunnelling[6]. In such experiments, the aim is to extract an electron from the wire with a given momentum, p. Such an electron would not be associated with a unique energy, $\varepsilon(p)$, owing to the interactions in the liquid, and would therefore leave behind multiple excitations (as above, the same considerations apply for holes and particles and, thus, for tunnelling from and into the wire). The probability of forming a state with energy ε if the added/extracted electron has momentum p is quantified by the spectral function, $A(p, \varepsilon)$. In 1D wires, this information can be obtained from momentum-conserving tunnelling between two parallel 1D electron channels formed in a semiconductor field-effect device[6–8,35]. In such a device, the momentum of the tunnelling electron is tuned using a magnetic field, B, applied perpendicular to the wires, and the energy resolution is achieved by controlling the interwire bias, V (Figs 2 and 3a), yielding information about the electron spectral function, $A(p, \varepsilon)$, through the interwire current, $I(B, V)$. A complication of this technique in comparison with, for example, angle-resolved photoemission spectroscopy[36,37] is the unavoidable electrostatic interaction between the wires. Because of this interaction, some effort is necessary to extract $A(p, \varepsilon)$ from the measurement of $I(B, V)$ (refs 6, 7).

Ideally, spin–charge separation would manifest itself as two peaks in the energy dependence of $A(p, \varepsilon)$ at a fixed value of p. For definiteness, we concentrate here on the case of p values slightly less than the Fermi momentum, p_F, and ε values less than zero, that is, on the probability of extracting a particle from a Luttinger liquid. Then, the two peaks signify the two extremes in sharing of the momentum by the elementary charge and spin excitations (holons and spinons, respectively[38]). The high-energy peak (with the largest value of $|\varepsilon|$) is located at $\varepsilon = v_\rho(p - p_F)$ and corresponds to the entire momentum being given to a holon. The low-energy peak, at $\varepsilon = v_s(p - p_F)$, corresponds to the entire momentum being carried away by a spinon (Fig. 3). This peak actually corresponds to the lowest-energy state of the Luttinger liquid, which may be created by removing from it a particle with momentum p; $A(p, \varepsilon)$ must equal zero for any smaller value of $|\varepsilon|$. For $|\varepsilon|$ values slightly above the threshold, $|v_s(p - p_F)|$, a small part of the hole's energy is spent on the creation of charge waves with small wavevectors, $|q| \ll |v_s(p - p_F)|/v_\rho$, and the greater part is carried by a spinon.

Luttinger liquid theory predicts that the two described peaks in the

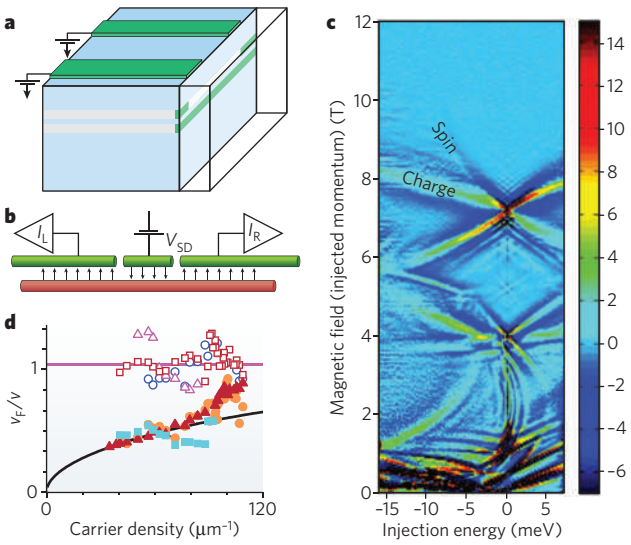

Figure 3 | Probing spin–charge separation and charge fractionalization in interacting 1D wires using momentum-resolved tunnelling spectroscopy. a, Schematic structure of the double-wire geometry, made using the cleaved-edge overgrowth technique[7]. The double-wire system resides at the edge of a gallium arsenide/aluminium gallium arsenide double-well structure. Dark green, gates; blue, AlGaAs; white, GaAs; light green, 1D wire segments; transparent box, epitaxial confining layer on the cleaved edge. **b**, Schematic of circuit used to measure the spectral function and charge fractionalization. I_L, left-moving current; I_R, right-moving current; V_{SD}, bias voltage. **c**, Measured spectral function, $\partial I(V, B)/\partial V$, indicating the spin and charge excitation branches (plotted versus injection energy, eV, on the horizontal axis). A smooth background has been subtracted from the data. The colour scale indicates the magnitude of $\partial I(V, B)/\partial V$ (arbitrary units). The features labelled spin and charge cross at zero energy at a magnetic field of around 7 T. **d**, Measured spin velocities (open symbols) and charge velocities (filled symbols) for different carrier densities (colours), plotted as the Fermi velocity, v_F, divided by the measured velocity, v. A lower carrier density corresponds to stronger repulsion between electrons and hence to a larger charge excitation velocity. The spin modes are nearly independent of the carrier density. Solid curves are theoretical fits. (Panel reproduced from ref. 6.)

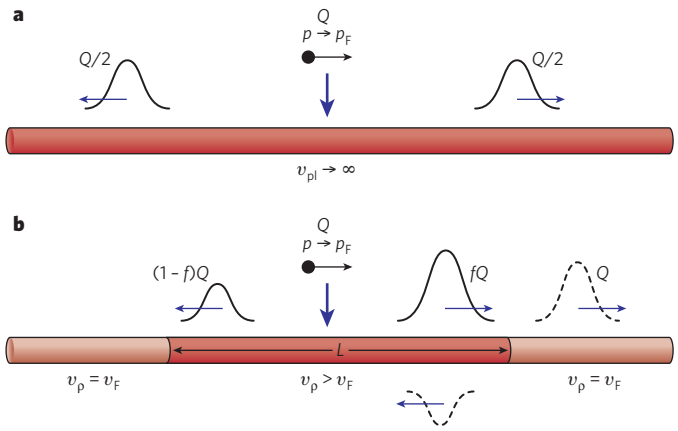

Figure 4 | Spreading of charge on tunnelling into an interacting wire. a, An electron liquid in a homogeneous infinite wire in the absence of shielding supports plasmons that transfer the tunnelled charge to the outer parts of the system; in the limit $v_{pl}/v_F \to \infty$, the initial momentum of the charge does not affect the pattern of transient charges. **b**, Transient charges at a finite charge mode velocity, v_ρ, in the presence of free-fermion leads. The charge pulse splits into transmitted and reflected components (dashed) at the boundary of two media with different 'refraction indices' for the charge waves. In the set-up shown, multiple reflections at the two boundaries result in the entire tunnelled charge, Q, being transferred into the right-hand lead and zero charge exiting into the left-hand lead.

electron spectral function are power-law singularities, with exponents defined by the strength of the inter-electron interaction[39]. Singular points in the energy–momentum plane form one pair of lines, $\varepsilon = v_\rho(p - p_F)$ and $\varepsilon = v_s(p - p_F)$, that intersect at $(0, p_F)$, and a similar pair that intersect at $(0, -p_F)$. In the experiment (Fig. 3), the momentum of a tunnelling electron is tuned using B and its maximal energy is determined using V. The intersecting straight lines tracing the singularities of $A(p, \varepsilon)$ correspond to the intersecting straight lines tracing the singularity in the differential conductance in the V–B plane.

Measurements[6,7] reveal clear maxima of $\partial I(V, B)/\partial V$ along a system of lines in the V–B plane, consistent with theory[40]. Two of the lines indeed form a crossing (see Fig. 3c, where the injection energy, eV, is plotted against B), at a point that can be unambiguously identified with the tunnelling of electrons with momenta approaching p_F. The velocities of the corresponding excitations can be extracted from the slopes of the two lines at the crossing point. These velocities are in reasonable agreement with theoretical estimates for the velocities of charge and spin modes (Fig. 3d). Current measurements are not accurate enough for to tell whether $\partial I(V, B)/\partial V$ is actually divergent along the lines corresponding to the spectra of the two modes.

Further recent work exploiting a similar idea, based on tunnelling between a wire array and a two-dimensional electron gas, also found multiple excitation velocities consistent with theory[41]. Taken together, experiments[6,7,41] provide direct confirmation of the phenomenon of spin–charge mode separation in 1D electron systems at low energies.

Although there is a qualitative agreement with the Luttinger liquid theory for momenta approaching p_F, the experiments on momentum-conserving tunnelling have sharpened a question that is not addressed within the Luttinger liquid theory, that of what happens to spin–charge separation at higher energies. The two experiments[6,7] do demonstrate that a remnant of the charge mode spectrum survives at higher bias, in the form of a parabolic dispersion relationship similar to a free-particle excitation. However, traces of the spin mode fade away at higher energies. Finding a theoretical answer to the question requires accounting for the nonlinearity of the generic electron spectrum, which necessitates going beyond the Tomonaga–Luttinger model, in which the linearity of the spectrum is a central assumption. Some suitable tools for developing a theory of a liquid of quantum particles with a generic dispersion relationship (a nonlinear Luttinger liquid) were found only recently[9,42,43] and several experimentally testable predictions have already been made, among them the survival of the power-law singularity of $A(p, \varepsilon)$ to higher energies for certain modes[43] and particle–hole asymmetry in the relaxation rates[10]. The second of these predictions can be tested using existing[6] experimental techniques. We return to the question of spin–charge separation at higher energies below.

Charge polarization and break-up

In the discussion of momentum-resolved tunnelling, we considered an idealization of an infinitely long junction between two parallel wires. In practice, the junction typically has a length of few micrometres, which is long on the scale of the Fermi wavelength and does not limit the use of momentum as a good quantum number[7]. Electrons with given momenta are injected near the middle of a long quantum wire (Fig. 3b). This poses the question of how the injected charge spreads once it is in the wire. Predictably, the answer depends on the circumstances, leading to interesting considerations related to the break-up, or 'fractionalization', of charges.

First, look at the ideal case of a quantum wire in the absence of any other conductors that may shield the electric field produced by charges in the wire. In this case, the dispersion relationship for the charge mode is $\omega(q) \approx q\sqrt{[\ln(1/wq)]}$, where w is the wire's width and q is the wavevector of the charge excitation, or plasmon. If the tunnelling electrons have low energies (such that their momenta are close to $\pm p_F$), then only low-energy plasmons can be excited. Such excitations have small wavevectors ($q \to 0$) and, thus, diverging velocities, $v_{pl} \approx \sqrt{[\ln(1/wq)]} \to \infty$. Relative to the plasmons, the velocity of a tunnelling electron, $v \to v_F$ (where v_F is the Fermi velocity), is so small that its direction is inconsequential; tunnelling of a charge Q with a well-defined momentum thus creates two pulses, each of charge $Q/2$, running in opposite directions (Fig. 4a). Although this is somewhat counterintuitive, it is no different from the dynamics of charge screening in higher dimensions: in a conducting liquid, a polarization charge develops that locally compensates the charge of the tunnelling electron and spreads it towards the edges of the system. An electron tunnelling into a two-dimensional electron liquid, for example, would create a circularly symmetric 'splash' of polarization charge.

Shielding of the long-range Coulomb forces reduces the infinite (for $q \to 0$) plasmon velocity, v_{pl}, to a finite velocity, v_ρ, of charge wave propagation. For a finite ratio v_ρ/v_F, the waves of polarization moving in opposite directions away from the tunnelling point differ from each other (Fig. 4b). The fraction, f, of the tunnelling charge, Q, that is carried by the wave propagating in the direction of the incident electron motion can be found from the momentum conservation law (for pedagogical reasons, it is better to consider the case in which $Q \gg e$). The momentum of the tunnelling charge, $(Q/e)mv_F$, is carried away by particles of the same mass, m, moving in opposite directions with velocity v_ρ. The momentum conservation law takes the form $fv_\rho - (1-f)v_\rho = v_F$, yielding $f = \frac{1}{2}(1 + v_F/v_\rho)$; in the absence of interactions ($v_\rho = v_F$), the expected result, $f = 1$, is obtained.

We should emphasize the distinction between the notions of charge quantization and fractionalization. Nowhere in the above discussion was a particular value of the tunnelling charge, Q, important, consistent with the idea of a liquid as a description of a continuous medium. The quantized value of the charge of the particles forming the liquid must come from a separate, microscopic consideration. (For example, the quantized fractional charge of quasiparticles under the conditions of the fractional quantum Hall effect is defined by the special properties of the corresponding microscopic wavefunction[44].)

This discussion of charge fractionalization is applicable as long as the polarization charges do not hit the ends or some other inhomogeneity of the wire. In principle, a direct determination of f can be achieved from a time-resolved measurement of the transient currents in the wire or from a measurement of the current noise spectrum[45]. However, d.c. measurements cannot determine f. This limitation is illustrated here in the simplest geometry of free-fermion leads attached to a Luttinger liquid of length L. The contact with the leads may be modelled as a smooth spatial variation of the charge wave's speed from v_ρ to v_F. Being smooth on the length scale set by the Fermi wavelength, such an inhomogeneity does not backscatter individual electrons; by analogy with optics, it rather acts as an interface of

two media with different refraction indices for the charge waves (Fig. 4b). To analyse the d.c. measurement, consider the propagation of charges over times much greater than that, L/v_ρ, needed to traverse the Luttinger liquid. The propagation occurs in the free-fermion part of the system. As the electrons do not backscatter, the momentum conservation law can be applied as was done above, but with the replacement $v_\rho \rightarrow v_F$. This leads to the conclusion that the entire tunnelled charge eventually ends up moving in the direction of the initial electron's momentum, regardless of the value of f within the Luttinger liquid (Fig. 4b).

The concept of charge fractionalization provides a convenient basis for calculations within Luttinger liquid theory. Experiments performed at low injection energy, using the more sophisticated configuration of a three-terminal d.c. measurement (Fig. 3b) with momentum-selective source and drains attached to the wire, are in excellent agreement with theory[8]. Such d.c. measurements can also be analysed within the framework of charge fractionalization, but they do not allow determination of f.

A natural question to ask is how the asymmetry between currents in the two drains (Fig. 3b) behaves at higher injection energies, once the conventional Luttinger liquid theory breaks down. Answering this question may provide information about the differences between the kinetics of injected high-energy particles and holes.

Nonlinear Luttinger liquid

To analyse the above-mentioned experiments, aimed at measuring the spectral functions of electrons and holes at higher energies and at elucidating how the injected charge propagates along the wire at these higher energies, it is necessary to go beyond conventional Luttinger liquid theory. There is also an impetus to do so from within the theory. The linearization of the particles' spectrum that is assumed in the Tomonaga–Luttinger model brings an immense degeneracy into the energy spectrum of the excited many-body states: the energy of a state composed of an arbitrary number of particle–hole pairs residing on one branch of the single-particle spectrum depends only on the total momentum of the pairs and is insensitive, for example, to the number of pairs. Reintroduction of the generic nonlinear dispersion relationship of the particles into the theory removes this degeneracy in a subtle way.

Recently, the nonlinear theory was developed for spinless quantum particles[9–11], and since then a first step has been made in generalizing the dynamic response theory to spin-½ fermions with a generic dispersion relationship[12,13]. The new methods make it possible to move beyond the linear Luttinger liquid description in understanding the dynamic response functions (such as the spectral function, $A(p, \varepsilon)$). They also provide a basis for understanding the kinetics of interacting quantum particles confined to one dimension, although the full kinetic theory has not yet been constructed. The new theory predicts the persistence of the power-law singularities in $A(p, \varepsilon)$ even for momenta far from the Fermi points and allows the evaluation of the corresponding exponents. In striking contrast to the conventional Luttinger liquid theory, it also predicts asymmetry in the relaxation rates for particles and holes.

Here we demonstrate the main idea of the new theory using the example of weakly interacting fermions without spin. Free particles have a parabolic dispersion relationship, $\varepsilon(p) = p^2/2m$, and here it is assumed that an equilibrium population of fermions occupies states with $|p| \leq p_F$. The focus is on evaluating $A(p, \varepsilon)$ for the hole excitations ($\varepsilon < 0$). In the absence of interactions, only one state of the system is created by extracting an electron with some momentum, p_0 ($-p_F \leq p_0 \leq p_F$), in the Fermi distribution; this state consists of a single hole with momentum p_0. The velocity of this hole, $|p_0|/m$, is less than v_F, which is the velocity of the lowest-energy particle–hole excitations. Therefore, interaction of this hole with the particles of the Fermi sea does not lead to creation of excitations, in much the same way that a particle moving at less than the speed of light in a medium does not emit Cherenkov radiation. This means that the existence of the energy threshold in $A(p, \varepsilon)$ along some line, $\varepsilon(p)$, at a momentum $|p| \leq p_F$ is robust with respect to the interaction (Fig. 5). At the same time, the functional form of $A(p, \varepsilon)$ is modified by interaction away from its free-fermion limit, $A(p, \varepsilon) \approx \delta(\varepsilon - \varepsilon(p))$ (where δ denotes the delta function). Remarkably, this modification is universal: the threshold behaviour of $A(p, \varepsilon)$ is described by a power-law function of $\varepsilon(p) - \varepsilon$, as in the Tomonaga–Luttinger model. Unlike in that model, however, the power-law behaviour at the threshold is valid at any momentum, and the exponent of the power law depends on the momentum.

To explain the power-law form of $A(p, \varepsilon)$, here we allude[46] to the effect known as the Anderson orthogonality catastrophe[47]. For definiteness, consider the part of $A(p, \varepsilon)$ associated with the creation of a hole in the system. The introduced hole produces a potential acting on other particles. The threshold in $A(p_0, \varepsilon)$ corresponds to the ground-state energy of the many-body system adjusted to that potential. The 'old' (pre-hole) and 'new' many-body ground states have zero overlap[47]. The overlap with excited states is finite and scales as some power of the excitation energy (measured relative to the new ground state). This non-zero overlap with excited states of the Fermi sea results in the redistribution of the spectral weight in $A(p_0, \varepsilon)$ from a single point ($\varepsilon = \varepsilon(p_0)$) to all energies above the threshold, according to a power law in $\varepsilon(p_0) - \varepsilon$.

This picture, which was initially developed for weakly interacting particles, has been extended into a fully consistent phenomenological theory[9,43] valid at arbitrary interaction strength. The phenomenology relates the threshold exponents of a dynamic correlation function to the properties of the corresponding threshold energy spectrum; these two types of characteristic can be measured independently of each other.

The limit of weakly interacting fermions also demonstrates the difference between the particles and holes. Particles move at velocities greater than v_F (Fig. 5), allowing the 'Cherenkov radiation' of particle–hole pairs; unlike holes, energetic particles do relax, producing multiple particle–hole pairs. Although particle–hole asymmetry has not yet been observed, experiments to explore such deviations from Luttinger liquid theory are underway.

Developing the nonlinear Luttinger liquid theory of spin-½ fermions is of special interest. Such a theory should cover the case of strong interactions keeping fermions 'in place' and thus suppressing their spin-exchange interaction and creating an almost flat band of spinon excitations.

Correlated-electron solid at low density

In the previous sections, we discussed theory and experiment in the regime where the charge density is large enough to ignore the strong correlations between the electron positions that develop when the electron density, n, becomes sufficiently low. These correlations emerge because although the long-range part of the electron–electron interaction chiefly affects the value of v_ρ, as this depends on the electrostatic energy required to create long-wavelength charge fluctuations, the increase of its short-range part ($\sim e^2 n$) relative to the single-electron

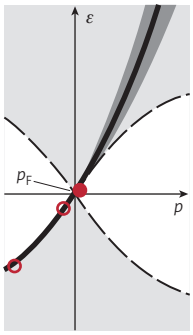

Figure 5 | Effects of the finite mass of particles forming the nonlinear Luttinger liquid. At positive curvature of the energy–momentum function, $\varepsilon(p)$ (solid black line), the velocity of a hole is less than v_F and therefore a hole state is stable, unlike a particle state (the particle spectrum is shown as the dark-grey broadened line). The spectrum of holes (dashed black lines) forms the threshold for the spectral function, $A(p, \varepsilon)$, which is finite everywhere in the light-grey shaded area. Creation of a 'deep' hole (lower open red circle) perturbs the Fermi sea, creating low-energy particle–hole pairs (open and filled red circles near the Fermi point); this process results in the power-law threshold singularities in $A(p, \varepsilon)$ discussed in the text.

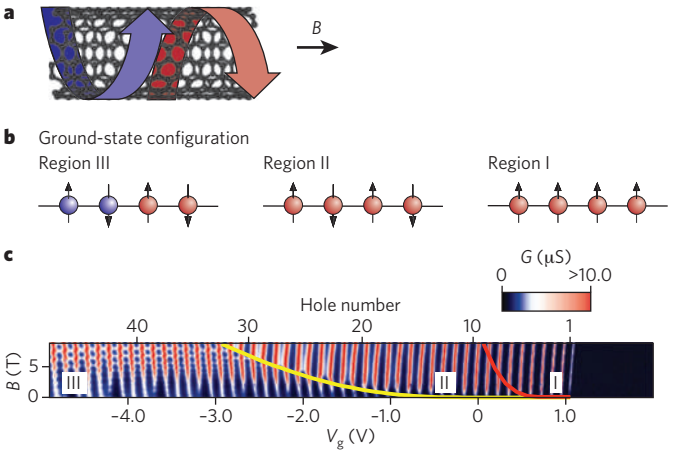

Figure 6 | Charges at low densities in a carbon nanotube form a 1D Wigner crystal. a, Although the sense of motion of electrons around the nanotube (red and blue arrows) depends on the direction of the magnetic field, *B*, in an armchair tube, in a tube of general chirality electrons with both senses of motion can be present. The sense of motion for each charge can be labelled using an isospin quantum number. **b**, Ground-state configurations of charges in the regions (I–III) described in the text. **c**, Differential conductance, *G*, of a nanotube as a function of gate voltage, V_g, and magnetic field. The vertical stripes are the traces of the conductance peaks. (Panel reproduced, with permission, from ref. 14.)

kinetic energy ($\sim\hbar n^2/m$, where $\hbar$ denotes Planck's constant divided by 2π and m denotes the electron mass) tends to suppress the electrons' ability to pass by each other. This produces a 1D Wigner-crystal-like structure with periodically ordered charges[48–52]. (Note that although perfect charge ordering in one dimension is not expected, the correlation length can readily exceed the sample length in realistic situations, yielding a state that is much more like an electron solid than an electron liquid.) For $e^2n \gg \hbar n^2/m$, the positional exchange between neighbouring electrons becomes exponentially rare and the fluctuations of their relative positions become small (the condition can be recast in the form $na_B \ll 1$, where a_B is the effective Bohr radius for a conduction electron in the material). The suppressed exchange decreases the spin mode stiffness, lowering the energy cost of spin excitations. If exchange is ignored entirely, the spin system becomes disordered for any positive temperature. This so-called spin-incoherent regime has been a topic of much recent theoretical interest[53].

Studying the properties of such a system requires low-disorder samples to avoid an insulating state where disorder pins the Wigner crystal. Potential clean systems in which to study such behaviour include wires made using cleaved-edge overgrowth[35] and semiconducting carbon nanotubes[54]. In particular, advances in sample preparation for carbon nanotubes have allowed the measurement of as-grown, suspended nanotubes, minimizing the tube–substrate interaction and producing very clean and low-disorder 1D systems that may reveal Wigner crystal physics. As discussed above, one of the hallmarks of a Wigner crystal state is that the antiferromagnetic exchange energy, *J*, is exponentially suppressed at low densities. This has an interesting consequence for the spin polarization in an external magnetic field. In contrast to free electrons, for which full polarization occurs only if the Zeeman energy, $g\mu_B B$ (where *B* is the magnetic field, μ_B is the Bohr magneton and *g* is the *g* factor), of an electron spin exceeds the Fermi energy, in a Wigner crystal polarization occurs at exponentially smaller fields, as only the condition $g\mu_B B > 2J$ is required.

In addition to their spin, electrons in nanotubes have an extra isospin degree of freedom, which is an additional angular momentum acquired by the electrons because of their motion around the axis of the nanotube (either clockwise or anticlockwise; Fig. 6a). In an axial magnetic field, the Zeeman effect splits the spin states[55,56] and their different orbital magnetic moments, $\pm\mu_{orb}$, split the isospin states[57]. The isospin splitting, $2\mu_{orb}B$, is typically larger than the Zeeman splitting by a factor of ~5–10 (ref. 57). The periodically ordered electrons forming the Wigner crystal act as a spin and isospin chain. For $B > 0$, the ground state reflects a competition between the magnetic energy, which favours parallel spins and parallel isospins, and the exchange energy, which favours neighbouring electrons having different spin and/or isospin directions[14,58].

Because *J* increases rapidly with *n*, in a magnetic field it is expected that there are three different regimes for a Wigner crystal state in a carbon nanotube as *n* and *B* are varied. In one (region I), the magnetic energy is dominant and all the electrons are fully spin and isospin polarized. In another (region II), the exchange dominates the Zeeman splitting but not the orbital splitting, which is larger, and only the isospin is polarized. In the last (region III), the exchange energy is dominant and the polarization is minimal for the given number of electrons. Figure 6b shows the ground-state configurations for these states.

Coulomb blockade spectroscopy provides a very useful tool to study this experimentally. In Coulomb blockade spectroscopy, the device acts as a single-electron transistor, producing peaks in the dependence of conductance on gate voltage, V_g, whenever an electron is added to the dot, thereby changing the electron density. The peak spacing reflects the energy required to add each electron. Because the magnetic energy contribution to this energy is different for each combination of quantum numbers, measurement of each peak's energy shift as a function of *B* yields the charges' quantum numbers. Figure 6c shows the evolution of the Coulomb peaks in a magnetic field for a semiconducting carbon nanotube, which displays all three regimes: in region I, the parallel traces that conductance peaks produce in the B–V_g plane indicate that each added electron has the same spin and isospin; in region II, the alternating slopes indicate that isospin is polarized and that spins alternate; and in region III, the zigzag pattern indicates the minimum polarization state[14].

The yellow line in Fig. 6c shows a single-parameter fit to theory[58], with the fitting parameter within the theoretically predicted range[58,59]. The red line is a plot of the boundary between regions I and II made using the same parameter value. The quantitative agreement with theory is satisfactory. We note that a model of non-interacting electrons predicts very few or no spin-polarized electrons under the same conditions[14].

The success of the Wigner crystal picture in accounting for the relative ease of polarizing electron spins in nanotubes in a magnetic field suggests that testing a theory[49] predicting one-half the usual conductance of a ballistic channel in the spin-incoherent regime would be very interesting. However, this would require progress in reliably obtaining nearly perfect contacts to ultraclean semiconducting nanotubes.

Mott insulator

The presence of enhanced spatial correlations between the electrons due to the interactions (that is, Wigner crystallization) increases the tendency towards pinning by inhomogeneities. When pinned, an electron system becomes insulating at sufficiently low temperatures. Suppression of conductance observed in gallium arsenide wires made using cleaved-edge overgrowth has been tentatively explained[35] in terms of such a pinning phenomenon.

The atomic lattice can be another source of pinning in an interacting electron system. Because of the lattice periodicity, pinning opens an energy gap in the electron spectrum. Commensurability between the mean electron spacing and the lattice period aids the opening of the gap. When electrons are on a lattice at half-filling (one conduction electron per atom), such a situation occurs. An example illustrating this is a 1D lattice-site chain in which a large energy cost, *U*, exists for double occupancy of a site and where the hopping matrix element, *t*, between sites can be considered small. At half-filling, every site is occupied, an electron–hole pair costs an energy *U* to create and the system is an insulator. This is essentially the physics of Mott insulators[60]. However, in contrast to 3D systems, where the formation of a Mott gap requires *U* to exceed some threshold, in one dimension a gap exists for any ratio $U/t > 0$.

Although such physics has been studied in bulk materials[61], carbon nanotubes afford the opportunity of potentially studying 1D Mott physics in an individual nanostructure with readily tunable parameters. Indeed, there is a puzzle to be solved — nanotubes predicted to

be metallic in the single-particle description are found experimentally to be gapped. Data taken from a so-called armchair nanotube (Fig. 6a) show such a gap (Fig. 7a) at zero doping. The simplest single-particle perturbations, such as curvature or strain of an armchair nanotube, are prohibited from opening a gap by symmetry constraints[62].

Such a gap may possibly be due to the many-body effect in Mott insulators. A number of works have included electron–electron interactions in theories of carbon nanotubes and found that the interactions should open a gap at half-filling[18,31–34]. The structure of a general nanotube is determined by a pair of integers (N, M), which specifies the tube's chirality and radius, r. For $N = M$, an 'armchair' nanotube (Fig. 6a), the honeycomb lattice can be mapped onto an equivalent 1D problem known as the two-leg ladder[31] (Fig. 7b). When long-ranged interactions are taken into account, theories predict an energy gap of $\Delta \approx 1/r^{\beta}$ for metallic nanotubes, with β ranging from $\beta = 1/(1-g)$ to $\beta = 2$ (ref. 63), depending on detailed assumptions. Here $g = v_F/v_\rho \approx 0.2$–$0.3$ for nanotubes[18,33] and is a measure of the strength of the interactions therein. Experiments show an approximate $1/r^{1.3}$ dependence[15], in agreement with the theoretical range of predicted values of the exponent.

Nevertheless, even in the most robust case of an armchair nanotube it remains possible that the observed gap originates from another single-particle perturbation, a twist. It is therefore beneficial to develop an approach that experimentally rules out the single-particle gap-opening mechanisms for nanotubes of arbitrary structure. Theory predicts that such gaps close at some value of an applied axial magnetic field and that a metallic state is recovered[62,64]. Interestingly, experiments performed on pristine, suspended carbon nanotubes show that the gap reaches a minimum, non-zero value at a critical magnetic field (~2.5 T for the device in Fig. 7c), before widening again[15]. The observation of a minimum gap rules out all of the above non-interacting theories of gap creation in these nanotubes.

Another indication of strongly interacting electrons in nanotubes comes from the presence of low-energy neutral electronic excitations with energies less than the gap energy[15]. (By contrast, if the electron system were non-interacting, the lowest-energy excitation would be that which moves an electron from the valence band to the conduction band, costing an energy equal to the gap energy.) Although the origin of these low-energy excitations is not yet fully understood, their presence is consistent with the Mott theory[31–34], which predicts neutral excitations of the Mott insulator with energies less than the gap energy, such as spin excitations, and an energy scale similar to that observed. This provides further evidence for a many-body origin of the observed gap in carbon nanotubes.

In future, signatures of a 1D Mott insulator around its metal–insulator transition point[65] may be investigated. Furthermore, the exotic spin liquid excitations predicted for carbon nanotubes[34] could be studied in detail. Finally, gaps could be opened even in the absence of pinning. It has been theorized for Wigner crystals[48] that in wider channels the 1D Wigner crystal will make a transition to a zigzag phase with a gapped mode, in addition to a gapless one, as its hallmark. Recent conductance measurements of wide quantum wires[66] are consistent with this picture; however, the gapped mode has not yet been directly observed.

Future directions

Further experiments, including those on systems and using techniques not discussed here, are expected to provide more insight into the nature of interacting particles confined to one dimension. Examples include experiments on cold-atom systems (see, for example, ref. 4) and time-resolved measurements of charge and spin dynamics (a recent experiment in carbon nanotubes[67] has yielded promising results; however, the fast charge mode has not yet been observed, possibly owing to insufficient time resolution). In addition to contributing to the understanding of the fundamental physics of excitons in one dimension[68–70], optics measurements may give new access to a broad range of quantum impurity problems (see, for example, ref. 71). One-dimensional systems may be controllably integrated with external structures such as an external periodic potential to create an artificial Mott insulator that can provide

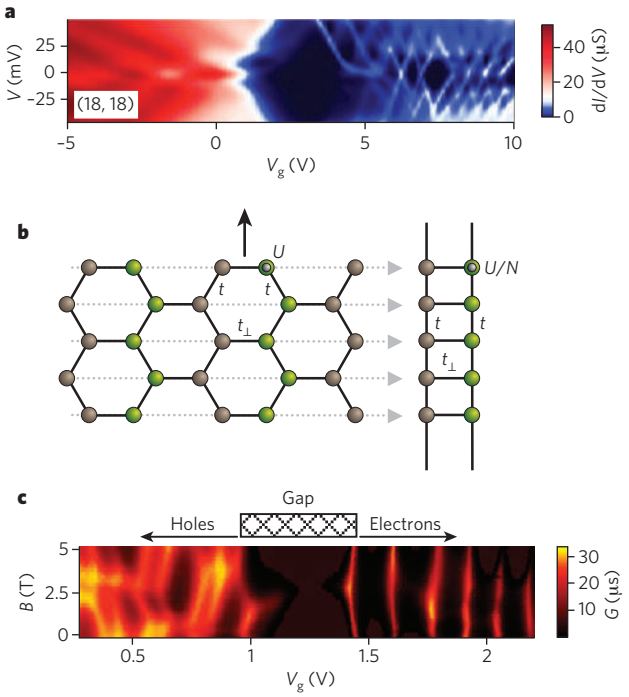

Figure 7 | Electron correlations in 1D carbon nanotubes give rise to insulating gaps. a, Colour plot of differential conductance, dI/dV, as a function of source–drain bias, V, and gate voltage, V_g, for an (18, 18) nanotube. The large region of dI/dV suppression near the centre indicates the presence of a gap. (Data courtesy of V.V.D., M. Takekoshi, P. Kim, J. Hone and T. Heinz.) **b**, Mapping of the honeycomb lattice onto an equivalent two-leg ladder system. Brown and green distinguish which atoms in the nanotube are mapped onto which ladder leg. The parameter U is the electronic on-site interaction discussed in the main text, and t and $t_\perp$ are the electron hopping matrix elements. The effective on-site interaction in the equivalent ladder is reduced by a factor N, to U/N, for an (N, N) nanotube. The black arrow indicates the tube's cylindrical axis. **c**, Conductance, G, as a function of magnetic field, B, and gate voltage, showing a gap that reaches a minimum value for $B \approx 2.5$ T. (Panel reproduced from ref. 15.)

a highly tunable means of harnessing many-body physics in the solid state and developing new applications such as a pump for quantized fractional charge[59]. A number of interesting theories[42,53] concerning spin-incoherent and nonlinear Luttinger liquids may be investigated.

There is also significant theoretical work ahead aimed at filling the gaps between the limits of the Tomonaga–Luttinger model and incoherent Luttinger liquids and between the limits of ideally ordered 1D interacting systems and general disordered ones. In the case of disordered Luttinger liquids, the recognized[72] need for further theory is driven by experiments with carbon nanotubes out of equilibrium[73] and by current theoretical predictions such as many-body localization[74]. Given the rapid evolution of its experimental and theoretical techniques, the field of correlated many-body 1D systems looks set for more exciting developments in the future. ■

1. Landau, L. D. & Lifshitz, E. M. *Course of Theoretical Physics* Vol. 9, 1–27 (Pergamon, 1980).
2. Kinoshita, T., Wenger, T. & Weiss, D. S. Observation of a one-dimensional Tonks–Girardeau gas. *Science* **305,** 1125–1128 (2004).
3. Paredes, B. *et al.* Tonks–Girardeau gas of ultracold atoms in an optical lattice. *Nature* **429,** 277–281 (2004).
4. Kinoshita, T., Wenger, T. & Weiss, D. S. A quantum Newton's cradle. *Nature* **440,** 900–903 (2006).
5. Clément, D., Fabbri, N., Fallani, L., Fort, C. & Inguscio, M. Exploring correlated 1D Bose gases from the superfluid to the Mott-insulator state by inelastic light scattering. *Phys. Rev. Lett.* **102,** 155301 (2009).
6. Auslaender, O. M. *et al.* Spin-charge separation and localization in one dimension. *Science* **308,** 88–92 (2005).
This paper reports the observation of the spin-charge separation using momentum-resolved electron tunnelling.

7. Auslaender, O. M. *et al.* Tunneling spectroscopy of the elementary excitations in a one-dimensional wire. *Science* **295,** 825–828 (2002).
8. Steinberg, H. *et al.* Charge fractionalization in quantum wires. *Nature Phys.* **4,** 116–119 (2008).
9. Imambekov, A. & Glazman, L. I. Universal theory of nonlinear Luttinger liquids. *Science* **323,** 228–231 (2009).
This paper describes the theory of momentum-resolved electron tunnelling into a liquid of particles with a generic (nonlinear) dispersion relationship.
10. Khodas, M., Pustilnik, M., Kamenev, A. & Glazman, L. I. Fermi-Luttinger liquid: spectral function of interacting one-dimensional fermions. *Phys. Rev. B* **76,** 155402 (2007).
11. Pereira, R. G., White, S. R. & Affleck, I. Spectral function of spinless fermions on a one-dimensional lattice. *Phys. Rev. B* **79,** 165113 (2009).
12. Pereira, R. G. & Sela, E. Coulomb drag from spin–charge coupling at zero magnetic field. Preprint at ⟨http://arxiv.org/abs/0911.1391⟩ (2009).
13. Schmidt, T. L., Imambekov, A. & Glazman, L. I. The fate of 1D spin–charge separation away from Fermi points. Preprint at ⟨http://arxiv.org/abs/0912.0326⟩ (2009).
14. Deshpande, V. V. & Bockrath, M. The one-dimensional Wigner crystal in carbon nanotubes. *Nature Phys.* **4,** 314–318 (2008).
15. Deshpande, V. V. *et al.* Mott insulating state in ultraclean carbon nanotubes. *Science* **323,** 106–110 (2009).
This paper reports the observation of energy gaps in nominally metallic carbon nanotubes, as well as the presence of low-energy neutral excitations within the gap that are interpreted using the theory of 1D Mott insulators.
16. Kane, C. L. & Fisher, M. P. A. Transport in a one-channel Luttinger liquid. *Phys. Rev. Lett.* **68,** 1220–1223 (1992).
This paper predicted the zero-bias anomalies in tunnelling into a Luttinger liquid.
17. Egger, R. & Gogolin, A. O. Effective low-energy theory for correlated carbon nanotubes. *Phys. Rev. Lett.* **79,** 5082–5085 (1997).
18. Kane, C., Balents, L. & Fisher, M. P. A. Coulomb interactions and mesoscopic effects in carbon nanotubes. *Phys. Rev. Lett.* **79,** 5086–5089 (1997).
19. Matveev, K. A. & Glazman, L. I. Coulomb blockade of tunnelling into a quasi-one-dimensional wire. *Phys. Rev. Lett.* **70,** 990–993 (1993).
20. Yao, Z., Postma, H. W. Ch., Balents, L. & Dekker, C. Carbon nanotube intramolecular junctions. *Nature* **402,** 273–276 (1999).
This paper reports the power-law behaviour of the end-to-end tunnelling conductance between carbon nanotubes, consistent with Luttinger liquid theory.
21. Postma, H. W. C., Jonge, M., Yao, Z. & Dekker, C. Electrical transport through carbon nanotube junctions created by mechanical manipulation. *Phys. Rev. B* **62,** R10653–R10656 (2000).
22. Bockrath, M. *et al.* Luttinger-liquid behaviour in carbon nanotubes. *Nature* **397,** 598–601 (1999).
This paper studies two geometries for electron tunnelling into carbon nanotubes and shows that the energy dependence of the tunnelling rate is consistent with the theoretical predictions.
23. Nazarov, Y. V. Coulomb blockade of tunneling in isolated junctions. *JETP Lett.* **49,** 126–128 (1989).
24. Devoret, M. H. *et al.* Effect of the electromagnetic environment on the Coulomb blockade in ultrasmall tunnel-junctions. *Phys. Rev. Lett.* **64,** 1824–1827 (1990).
25. Girvin, S. M., Glazman, L. I., Jonson, M., Penn, D. R. & Stiles, M. D. Quantum fluctuations and the single-junction Coulomb blockade. *Phys. Rev. Lett.* **64,** 3183–3186 (1990).
26. Auslaender, O. M. *et al.* Experimental evidence for resonant tunneling in a Luttinger liquid. *Phys. Rev. Lett.* **84,** 1764–1767 (2000).
27. Postma, H. W. C., Teepen, T., Yao, Z., Grifoni, M. & Dekker, C. Carbon nanotube single-electron transistors at room temperature. *Science* **293,** 76–79 (2001).
28. Ilani, S., Donev, L. A. K., Kindermann, M. & McEuen, P. L. Measurement of the quantum capacitance of interacting electrons in carbon nanotubes. *Nature Phys.* **2,** 687–691 (2006).
29. Venkataraman, L., Hong, Y. S. & Kim, P. Electron transport in a multichannel one-dimensional conductor: molybdenum selenide nanowires. *Phys. Rev. Lett.* **96,** 076601 (2006).
30. Bachtold, A. *et al.* Suppression of tunneling into multiwall carbon nanotubes. *Phys. Rev. Lett.* **87,** 166801 (2001).
31. Balents, L. & Fisher, M. P. A. Correlation effects in carbon nanotubes. *Phys. Rev. B* **55,** R11973–R11976 (1997).
32. Krotov, Y. A., Lee, D. H. & Louie, S. G. Low energy properties of (*n*, *n*) carbon nanotubes. *Phys. Rev. Lett.* **78,** 4245–4248 (1997).
33. Odintsov, A. A. & Yoshioka, H. Universality of electron correlations in conducting carbon nanotubes. *Phys. Rev. B* **59,** R10457–R10460 (1999).
34. Nersesyan, A. A. & Tsvelik, A. M. Coulomb blockade regime of a single-wall carbon nanotube. *Phys. Rev. B* **68,** 235419 (2003).
35. Steinberg, H. *et al.* Localization transition in a ballistic quantum wire. *Phys. Rev. B* **73,** 113307 (2006).
36. Kim, B. J. *et al.* Distinct spinon and holon dispersions in photoemission spectral functions from one-dimensional $SrCuO_2$. *Nature Phys.* **2,** 397–401 (2006).
37. Damascelli, A., Hussain, Z. & Shen, Z.-X. Angle-resolved photoemission studies of the cuprate superconductors. *Rev. Mod. Phys.* **75,** 473–541 (2003).
38. Giamarchi, T. *Quantum Physics in One Dimension* 81–86 (Oxford Univ. Press, 2004).
39. Voit, J. One-dimensional Fermi liquids. *Rep. Prog. Phys.* **58,** 977–1116 (1995).
40. Carpentier, D., Peça, C. & Balents, L. Momentum-resolved tunneling between Luttinger liquids. *Phys. Rev. B* **66,** 153304 (2002).
41. Jompol, Y. *et al.* Probing spin–charge separation in a Tomonaga–Luttinger liquid. *Science* **325,** 597–601 (2009).
42. Pustilnik, M., Khodas, M., Kamenev, A. & Glazman, L. I. Dynamic response of one-dimensional interacting fermions. *Phys. Rev. Lett.* **96,** 196405 (2006).
43. Imambekov, A. & Glazman, L. I. Phenomenology of one-dimensional quantum liquids beyond the low-energy limit. *Phys. Rev. Lett.* **102,** 126405 (2009).
44. Laughlin, R. B. Anomalous quantum Hall effect: an incompressible quantum fluid with fractionally charged excitations. *Phys. Rev. Lett.* **50,** 1395–1398 (1983).
45. Berg, E., Oreg, Y., Kim, E. A. & von Oppen, F. Fractional charges on an integer quantum Hall edge. *Phys. Rev. Lett.* **102,** 236402 (2009).
46. Pustilnik, M. Dynamic structure factor of the Calogero–Sutherland model. *Phys. Rev. Lett.* **97,** 036404 (2006).
47. Anderson, P. W. Infrared catastrophe in Fermi gases with local scattering potentials. *Phys. Rev. Lett.* **18,** 1049–1051 (1967).
48. Meyer, J. S. & Matveev, K. A. Wigner crystal physics in quantum wires. *J. Phys. Condens. Matter* **21,** 023203 (2009).
49. Matveev, K. A. Conductance of a quantum wire in the Wigner-crystal regime. *Phys. Rev. Lett.* **92,** 106801 (2004).
50. Schulz, H. J. Wigner crystal in one dimension. *Phys. Rev. Lett.* **71,** 1864–1867 (1993).
51. Averin, D. V. & Nazarov, Y. V. Tunneling to and from the one-dimensional Wigner lattice. *Phys. Rev. B* **47,** 9944–9947 (1993).
52. Glazman, L. I., Ruzin, I. M. & Shklovskii, B. I. Quantum transport and pinning of a one-dimensional Wigner crystal. *Phys. Rev. B* **45,** 8454–8463 (1992).
53. Fiete, G. A. The spin-incoherent Luttinger liquid. *Rev. Mod. Phys.* **79,** 801–820 (2007).
54. Cao, J., Wang, Q. & Dai, H. Electron transport in very clean, as-grown suspended carbon nanotubes. *Nature Mater.* **4,** 745–749 (2005).
55. Cobden, D. H., Bockrath, M., McEuen, P. L., Rinzler, A. G. & Smalley, R. E. Spin splitting and even-odd effects in carbon nanotubes. *Phys. Rev. Lett.* **81,** 681–684 (1998).
56. Tans, S. J., Devoret, M. H., Groeneveld, R. J. A. & Dekker, C. Electron–electron correlations in carbon nanotubes. *Nature* **394,** 761–764 (1998).
57. Minot, E. D., Yaish, Y., Sazonova, V. & McEuen, P. L. Determination of electron orbital magnetic moments in carbon nanotubes. *Nature* **428,** 536–539 (2004).
58. Levitov, L. S. & Tsvelik, A. M. Narrow-gap Luttinger liquid in carbon nanotubes. *Phys. Rev. Lett.* **90,** 016401 (2003).
59. Novikov, D. S. Electron properties of carbon nanotubes in a periodic potential. *Phys. Rev. B* **72,** 235428 (2005).
60. Mott, N. F. Metal-insulator transition. *Rev. Mod. Phys.* **40,** 677–683 (1968).
61. Dagotto, E. & Rice, T. M. Surprises on the way from one- to two-dimensional quantum magnets: the ladder materials. *Science* **271,** 618–623 (1996).
62. Charlier, J., Blase, X. & Roche, S. Electronic and transport properties of nanotubes. *Rev. Mod. Phys.* **79,** 677–732 (2007).
63. Chen, W., Andreev, A. V., Tsvelik, A. M. & Dror, O. Twist instability in strongly correlated carbon nanotubes. *Phys. Rev. Lett.* **101,** 246802 (2008).
64. Yang, L., Anantram, M. P., Han, J. & Lu, J. P. Band-gap change of carbon nanotubes: effect of small uniaxial and torsional strain. *Phys. Rev. B* **60,** 13874–13878 (1999).
65. Garst, M., Novikov, D. S., Stern, A. & Glazman, L. I. Critical conductance of a one-dimensional doped Mott insulator. *Phys. Rev. B* **77,** 035128 (2008).
66. Hew, W. K. *et al.* Incipient formation of an electron lattice in a weakly confined quantum wire. *Phys. Rev. Lett.* **102,** 056804 (2009).
67. Zhong, Z., Gabor, N. M., Sharping, J. E., Gaeta, A. L. & McEuen, P. L. Terahertz time-domain measurement of ballistic electron resonance in a single-walled carbon nanotube. *Nature Nanotechnol.* **3,** 201–205 (2008).
68. Lefebvre, J. & Finnie, P. Polarized photoluminescence excitation spectroscopy of single-walled carbon nanotubes. *Phys. Rev. Lett.* **98,** 167406 (2007).
69. Wang, F., Dukovic, G., Brus, L. E. & Heinz, T. F. The optical resonances in carbon nanotubes arise from excitons. *Science* **308,** 838–841 (2005).
70. Maultzsch, J. *et al.* Exciton binding energies in carbon nanotubes from two-photon photoluminescence. *Phys. Rev. B* **72,** 241402 (2005).
71. Balents, L. X-ray-edge singularities in nanotubes and quantum wires with multiple subbands. *Phys. Rev. B* **61,** 4429–4432 (2000).
72. Gutman, D. B., Gefen, Y. & Mirlin, A. D. Tunneling spectroscopy of Luttinger-liquid structures far from equilibrium. *Phys. Rev. B* **80,** 045106 (2009).
73. Chen, Y.-F., Dirks, T., Al-Zoubi, G., Birge, N. O. & Mason, N. Nonequilibrium tunneling spectroscopy in carbon nanotubes. *Phys. Rev. Lett.* **102,** 036804 (2009).
74. Basko, D. M., Aleiner, I. L. & Altshuler, B. L. Possible experimental manifestations of the many-body localization. *Phys. Rev. B* **76,** 052203 (2007).
75. Tomonaga, S. Remarks on Bloch's method of sound waves applied to many-fermion problems. *Prog. Theor. Phys.* **5,** 544–569 (1950).
76. Luttinger, J. M. An exactly soluble model of a many-fermion system. *J. Math. Phys.* **4,** 1154–1162 (1963).

Acknowledgements A.Y. and L.I.G. acknowledge a discussion with B. I. Halperin of the difference between charge fractionalization and quantization. L.I.G. acknowledges support from the US National Science Foundation (NSF) Division of Materials Research (grant no. DMR-0906498) and the Nanosciences Foundation at Grenoble, France. M.B. acknowledges the US Office of Naval Research. A.Y. is supported by the NSF under contract DMR-0707484.

Author Information Reprints and permissions information is available at www.nature.com/reprints. The authors declare no competing financial interests. Correspondence should be addressed to M.B. (marc.bockrath@ucr.edu).